PHILOSOPHICAL TRANSACTIONS OF THE ROYAL SOCIETY A MATHEMATICAL, PHYSICAL & ENGINEERING SCIENCES

Reversal models from dynamo calculations

Graeme R. Sarson

Phil. Trans. R. Soc. Lond. A 2000 **358**, 921-942
doi: 10.1098/rsta.2000.0567

THE ROYAL SOCIETY

Reversal models from dynamo calculations

By Graeme R. Sarson†

School of Mathematical Sciences, University of Exeter, Exeter EX4 4QE, UK

A numerical model of convection driven dynamo action, exhibiting a dominantly dipole magnetic field subject to intermittent reversals, is described. This model was originally restricted to two azimuthal modes, but has now been extended towards full three-dimensional resolution. The hydrodynamic state of this model is explained by a thermal wind mechanism, which generates strong zonal flows and secondary meridional circulation from a characteristic temperature profile consistent with highly supercritical convection. The zonal flows generate strong zonal magnetic fields via an ω-effect, and the equilibration of the dynamo relies heavily on a reduction in this effect, as might be parametrized as an 'ω-quenching'. The time-behaviour of the model is complex, but the importance of meridional circulation in this respect is clear; fluctuations in this component of flow provide a simple kinematic mechanism for reversals. Some parallels between model solutions and geomagnetic observations are noted, although detailed comparisons remain premature. Although the model remains far from the appropriate physical regime, the thermal wind and kinematic reversal mechanisms described are quite general, and may continue to play a role in the geodynamo.

Keywords: geodynamo; reversals; computational models

1. Introduction

With the general acceptance of the magnetohydrodynamic (MHD) dynamo model for the maintenance of the geomagnetic field, the phenomenon of field reversals (and long term secular variation) presents no conceptual difficulties. There is no obvious reason why the fluid system in the Earth's core—presumably chaotically fluctuating, like other geophysical fluid systems—should prefer magnetic fields of a given parity, or prohibit events involving parity reversals. Indeed, the existence of reversals, and secular variation in general, was historically one of the strongest factors in favour of the dynamo explanation for the geomagnetic field.

While the theoretical possibility of reversals is quite clear, we would like to understand the phenomenon in a more quantitative way. Just as we would like to know which features of the fluid flow in the Earth's core can sustain a large-scale magnetic field, we would like also to know which features of the system contribute to the time-behaviour observed: what features of the MHD regime of the geodynamo are prone to, 'trigger', or are influenced by field reversals?

With the advent of widely available computing power, detailed numerical modelling of MHD dynamo processes is becoming feasible (although there remain many

† Present address: School of Mathematics and Statistics, University of Newcastle, Newcastle NE1 7RU, UK.

unsatisfactory features in all numerical models to date). Any numerical model for the geodynamo must be amenable to testing against the available (or feasible future) observations. Given the long time-scales over which the dynamo processes operate, and the comparative brevity of the historical geomagnetic record, the palaeomagnetic record—theoretically spanning billions of years, and giving both reversal and long term palaeosecular variation information—presents arguably the best hope for testing numerical models. This is particularly true given the possibility that the historical field is in an unrepresentative state; the present day field intensity may be twice that of the long term palaeomagnetic average (Juarez *et al*. 1998; Tauxe, this issue), a fact which might have major consequences for geodynamo models.

It should theoretically be possible to compare synthetic records (from numerical simulations) with the palaeomagnetic record, to test the validity of our models. Formidable difficulties with such a scheme exist, however. The current numerical models—even with their physical simplifications, and their remoteness from the geophysically relevant parameter regimes—cannot practically produce synthetic time-series longer than of order one million years. It is not clear that this is sufficient to allow any meaningful statistical description that might be compared with the palaeodata.

Furthermore, there are still many uncertainties associated with the palaeomagnetic record. The prevailing view, whereby reversals and excursions are thought to be more-or-less exceptional events, in a field characterized by long periods of stable polarity (Jacobs 1994), has been challenged by some recent studies (Langereis *et al*. 1997; Lund *et al*. 1998; Gubbins 1999), which present an alternative model characterized by frequent events, at least within the last million years. If this latter view proves tenable, and can be extended throughout the palaeomagnetic record, the implications for dynamo models may be great.

Numerical models can at least be run for long enough to produce isolated synthetic reversals, and the detailed physics behind those events can be studied. In terms of such isolated events, however, the palaeomagnetic record is rather restricted, with the limited accuracy of dating, compared with the relative rapidity of such transitions, resulting in only uncorrelated and highly site-dependent records being available for any given event. Current comparisons between numerical models and observations must therefore remain rather limited.

The aims of the current paper are perhaps more limited still. We focus on the behaviour of one simple numerical model, making no real claims for geophysical verisimilitude. Our numerical system and typical solutions are described (in §§ 2, 3), and the dynamo action is discussed, in terms both of the 'normal' sustenance of field, and of the reversal behaviour obtained (§ 4). Some geomagnetic (or palaeomagnetic) diagnostics are then calculated (in § 5), although we stress the prematurity of any detailed comparisons. The relevance of our model to the Earth is finally discussed (§ 6), in light of the limitations of our study; those features which are expected to be robust are emphasized.

2. The numerical system

We consider the simplest self-consistent system capable of dynamo action and amenable to numerical study, in the appropriate geometry for the geodynamo: a shell of self-gravitating, electrically conducting, Boussinesq fluid, rotating about the polar

(z) axis in spherical (r, θ, ϕ) geometry. The appropriate non-dimensional equations are then

$$\mathbf{e}_z \times \mathbf{U} - E\nabla^2\mathbf{U} = -\operatorname{grad} P + qRa\Theta\mathbf{r} + (\nabla \times \mathbf{B}) \times \mathbf{B}, \tag{2.1}$$

$$\frac{\partial \mathbf{B}}{\partial t} = \nabla \times (\mathbf{U} \times \mathbf{B}) + \nabla^2\mathbf{B}, \tag{2.2}$$

$$\frac{\partial \Theta}{\partial t} = -\mathbf{U} \cdot \operatorname{grad} \Theta + q\nabla^2\Theta, \tag{2.3}$$

$$\nabla \cdot \mathbf{U} = \nabla \cdot \mathbf{B} = 0, \tag{2.4}$$

in terms of the Ekman, Roberts and modified Rayleigh numbers

$$E = \frac{\nu}{2\Omega\mathcal{L}^2}, \qquad q = \frac{\kappa}{\eta}, \qquad Ra = \frac{g\alpha\beta\mathcal{L}^2}{2\Omega\kappa}, \tag{2.5}$$

given by the kinematic viscosity ν, rotation rate Ω, characteristic length-scale $\mathcal{L}$, thermal diffusivity κ, magnetic diffusivity η, gravitational acceleration g, coefficient of thermal expansion α, and mean radial temperature gradient β. $\mathbf{e}_z$ is the unit vector in the z-direction.

We have dropped the inertial terms in the momentum equation, consistent with the expected magnetostrophic force balance, i.e. we have taken zero Rossby number: $Ro = \eta/(2\Omega\mathcal{L}^2) = 0$. Despite the equally small viscosity expected for the core, we retain a finite Ekman number, however; the numerical difficulties associated with setting E to zero are well documented (Fearn 1994).

We use an inner core whose radius is one-third that of the outer core, so that our non-dimensional fluid shell is given by $1/2 < r < 3/2$. We use no-slip boundary conditions on $\mathbf{U}$, with the inner core free to rotate under viscous and magnetic torques. $\mathbf{B}$ is matched to an external potential field, and solved explicitly within the inner core. A fixed heat flux is imposed at the inner core boundary, this being the only heat-source present: fixed temperature is imposed at the outer boundary.

This basic model is described in more detail in Jones *et al.* (1995) and Sarson *et al.* (1998). The present work differs from the preceding in relaxing somewhat the severely limited azimuthal resolution previously used. To allow a tractable system at relatively low computational cost, the '$2\frac{1}{2}$-dimensional' approximation was originally used, whereby only the axisymmetric field and a single mode of the non-axisymmetric field were considered. (Each mode being a single wavenumber m in a harmonic expansion in azimuth of the form $\mathrm{e}^{\mathrm{i}m\phi}$.) We now consider M non-axisymmetric modes in general, retaining the base wavenumber $m = 2$ used in most previous calculations. In this paper, we report on calculations with $M = 2$ (i.e. wavenumbers $m = 0, 2, 4$) and $M = 4$ ($m = 0, 2, 4, 6, 8$). While clearly remaining of limited azimuthal resolution, these solutions allow some consideration of the effect of the original ($M = 1$) truncation on our solutions. The effect of odd subharmonics ($m = 1, 3, 5, \dots$) will be examined in future.

All variables are expanded in associated Legendre functions, $P_l^m(\cos\theta)$, and in Chebyshev polynomials, $T_n[x(r)]$. In the calculations detailed here, a minimum of 32 Chebyshev polynomials and 48 Legendre functions have been employed for each azimuthal mode. (Consistent solutions have been obtained with higher resolution in r and θ.) The current calculations impose no special equatorial symmetry. A pseudo-spectral method is adopted, and adaptive time-stepping is employed within

an $O(\delta t^2)$-accurate scheme: this is semi-implicit (Crank–Nicholson) for linear terms, explicit for nonlinear terms.

Hyperdiffusivities are employed in all three equations, following Glatzmaier & Roberts (1995*b*):

$$\nabla^2 \equiv (1 + \lambda l^3)\nabla^2, \tag{2.6}$$

where l is the degree of the relevant Legendre function $P_l^m(\cos\theta)$. Although the use of hyperdiffusivities is problematical (Zhang & Jones 1997; Zhang *et al*. 1998), they currently remain essential in allowing lower diffusive parameters (E and q) to be attained, at least for the longest length-scales. For a given E and q, they also allow higher Ra, and hence more strongly supercritical solutions, to be attained.

3. Dynamo solutions

The types of solutions obtained in different parameter regimes were discussed by Sarson *et al*. (1998) and are shown schematically in figure 1. At relatively high E and q, convection is dominated by non-axisymmetric columnar rolls: 'Busse–Zhang' type behaviour. For high E, such convection can be obtained at relatively low Ra (the critical Rayleigh number for non-magnetic convection, Ra_c, goes as $E^{-1/2}$ at small E), and the solutions are well-behaved, both temporally and spatially. At values of q of order 1 or greater, these relatively low values of Ra are sufficient to give reasonable values of the magnetic Reynolds number, $R_m = \mathcal{U}\mathcal{L}/\eta$, and so dynamo action is possible. Solutions broadly conforming to this type have been found in three-dimensional calculations by many groups; for a recent survey, see Jones (this issue). At lower values of E and q, (currently attained only using hyperdiffusivities, and so strictly applying only to the largest scale features), higher values of Ra are required, to give convection at all, and to give R_m sufficient to sustain a dynamo. Solutions in this regime are rather different, being dominated by axisymmetric flow and field, concentrated near the inner core: 'Glatzmaier–Roberts' type behaviour. Solutions of this basic type have been reported in detail in a series of papers by Glatzmaier & Roberts (1995*a*, *b*, 1996*a*, *b*, 1997) and Glatzmaier *et al*. (1999).

Locations of typical 'end-members' of these two types of solution are marked on figure 1, although the boundary between their two domains is somewhat imprecise. It should be noted, for example, that GR type behaviour can be obtained at relatively high E and q, if the system is driven sufficiently hard ($Ra \gg Ra_c$); the solutions described in this paper are at $E = 10^{-4}$, $q = 1$, although similar solutions have been obtained (at greater computational expense) at lower values of both parameters.

The extension to several azimuthal modes ($1 < M \leqslant 4$) does not appear to affect the essential nature of the dynamo solutions in either regime. For many BZ solutions, a significant component of energy is often found at the highest wavenumber included, and so the solutions are clearly not yet resolved in azimuth; nevertheless, the axisymmetric fields generated often appear similar (this being the whole motivation for the $M = 1$ approximation in the first place). (It should also be noted that some cases have been found where the energy spectra gives hope for numerical convergence; Jones (this issue) reports one such case.) For the GR solutions, the situation is more satisfactory, with the energy in each mode typically decreasing monotonically with wavenumber m, and the axisymmetric structure remaining very consistent. For this

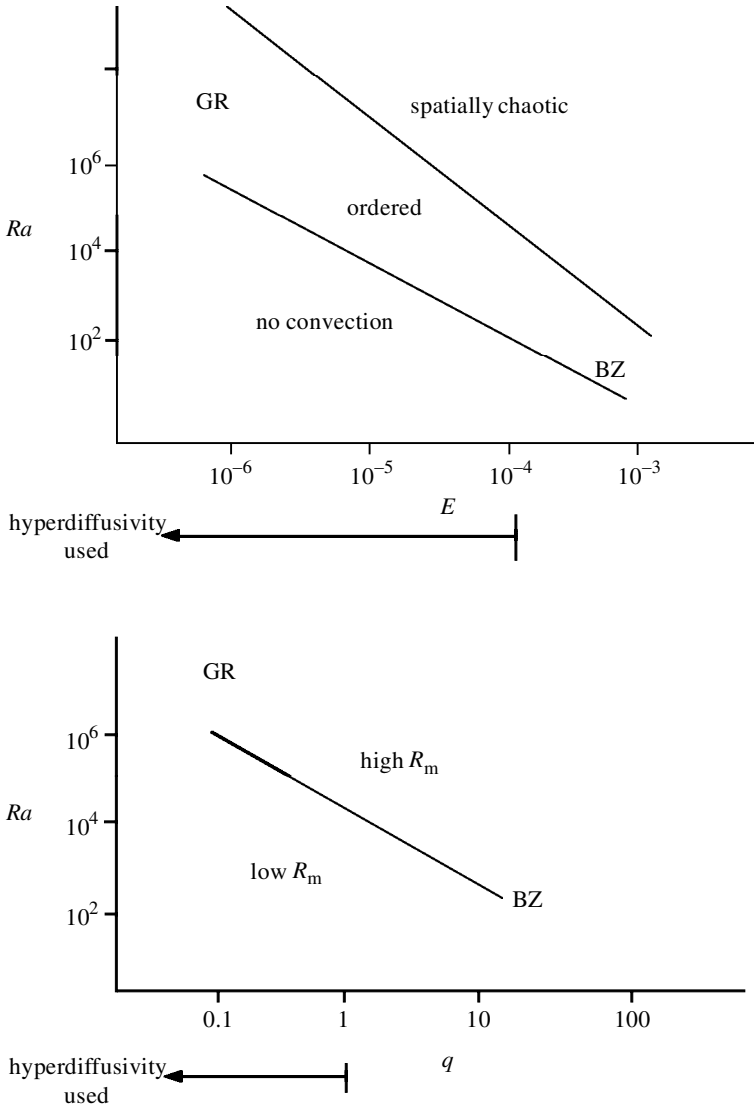

Figure 1. Schematic of the different regimes of parameter space. Dynamo action is only possible with high R_m convection. BZ and GR locate typical solutions of 'Busse–Zhang' and 'Glatzmaier–Roberts' type.

reason, and since these solutions exhibit reversal behaviour more appropriate for the geodynamo than the BZ solutions, we concentrate here on solutions of GR type.

The GR solutions maintain a field of fixed polarity for most of the time, with only occasional reversals being obtained. This can be seen from a time-sequence of the leading order coefficients of the dipole symmetry axisymmetric field (figure 2), for a solution obtained with $Ra = 45\,000$, $q = 1$, $E = 10^{-4}$, $\lambda = 0.05$, $M = 4$. This behaviour is essentially unchanged from the $M = 1$ ($2\frac{1}{2}$-dimensional) case described by Sarson & Jones (1999); this particular solution is at rather high Ra, and hence rather susceptible to reversals. The relative insensitivity of these solutions to M is

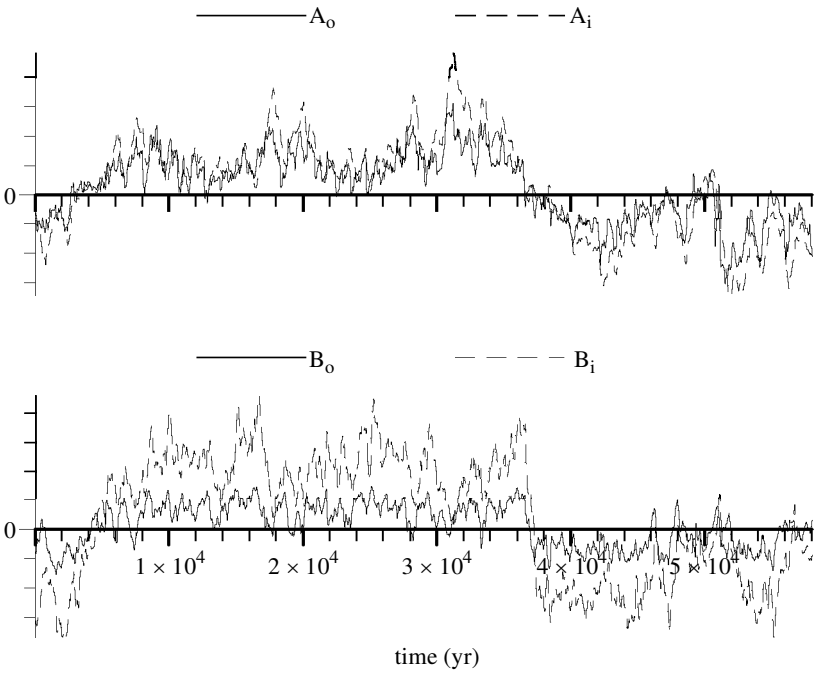

Figure 2. Time evolution of the leading coefficients of axisymmetric poloidal (A) and toroidal (B) field in the inner (i) and outer (o) cores, for a solution with $Ra = 45\,000$, $q = 1$, $E = 10^{-4}$, $\lambda = 0.05$, $M = 4$.

indicated in plots of the magnetic energy by wavenumber m, from runs with varying M; figure 3 shows the evolution of this quantity during representative time-intervals. For all three M considered, the axisymmetric field dominates, and the energy spectra essentially decrease monotonically with m. These facts, together with the observation that the solution morphology does not appear to differ fundamentally for different M, give us grounds for optimism as to the numerical validity of our solutions. Plots of kinetic energy provide a similar result, although the decay with wavenumber m is slightly less pronounced in that case. (To facilitate comparison with the Earth, we have here scaled our non-dimensional calculations to dimensional units, using typically quoted estimates for certain of the core physical parameters. In particular, we have scaled time by the magnetic diffusion time-scale, $\mathcal{T} = \mathcal{L}^2/\eta \sim 60\,000$ yr, and magnetic field strength by the magnetic scale, $\mathcal{B} = (2\Omega\rho\mu\eta)^{1/2} \sim 2.2$ mT. In most of this following, however, we will revert to non-dimensional units. Appropriate dimensional units can be obtained, if desired, by scaling non-dimensional magnetic fields as above, and non-dimensional velocities by the velocity scale $\mathcal{U} = \mathcal{L}/\mathcal{T} \sim 0.037$ km yr$^{-1} = 1.2 \times 10^{-6}$ m s^{-1}.)

A snapshot of the velocity of this solution can be seen in figure 4, which shows the vertical velocity (contours) and horizontal velocity (arrows) in the plane $z = 0.3$, parallel with the Equator, in the Northern Hemisphere. (Throughout this paper, we define vertical and horizontal to be parallel and perpendicular to $\mathbf{e}_z$, respectively; radial and tangential are defined to be parallel and perpendicular to $\mathbf{e}_r$.) The dominance of the zonal flow within the inner core tangent cylinder is apparent in the strong horizontal flows, just outside the inner core in this slice (at cylindrical radius

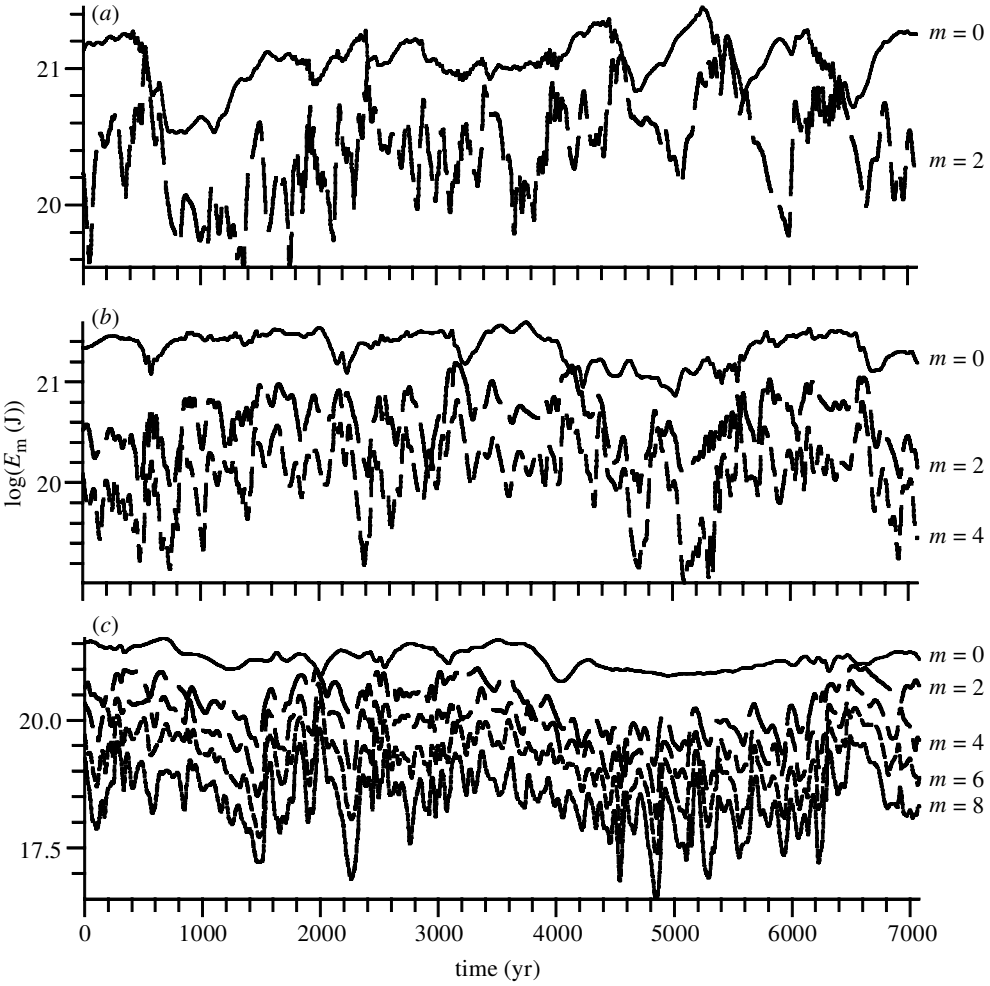

Figure 3. Time evolution of magnetic energy, subdivided by azimuthal wavenumber m, for solutions with $Ra = 45\,000$, $q = 1$, $E = 10^{-4}$, $\lambda = 0.05$, with $M = 1$, 2 and 4 ((*a*), (*b*) and (*c*), respectively).

$s = 0.4$). Although smaller than the zonal flow, the non-axisymmetric convection outside the tangent cylinder remains strong, convecting heat outwards efficiently (the zonal flow transports no heat, and the axisymmetric poloidal flow is rather small in this region). This component of convection is strongest in the vicinity of the inner core, as is typical (and might be expected) for convection driven by an imposed heat flux there (cf. uniform internal heating). The non-axisymmetric convection remains rather columnar; in contrast to the BZ type columns, however, these structures are not long-lived, but fluctuate rather chaotically (and may drift in either direction).

The axisymmetric state of this solution, at the same instant, is shown in figure 5. The structure of the zonal flow can now be seen in the angular velocity $v/(r\sin\theta)$. The axisymmetric poloidal flow can be seen from the quantity $\psi r\sin\theta$, which is a streamfunction for the meridional circulation; flow is clockwise around positive contours, and the dominant flow here constitutes a single large-scale cell, flow being

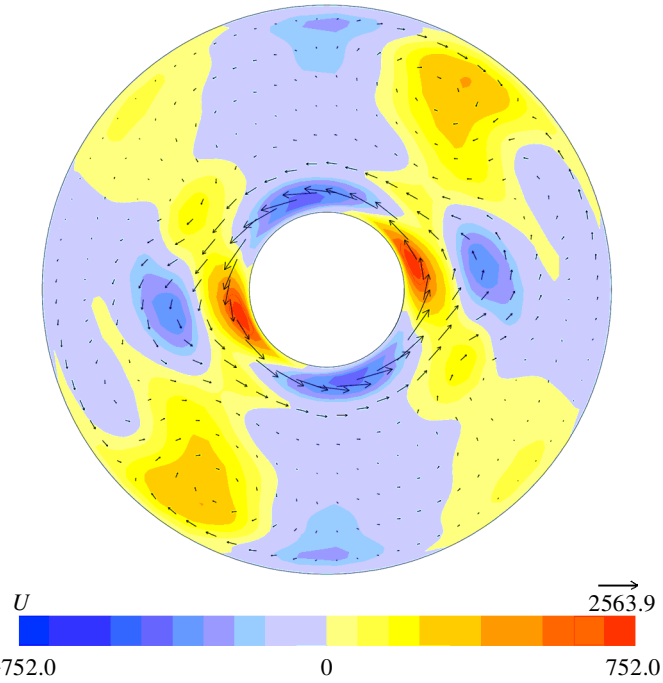

Figure 4. Velocity in slice $z = 0.3$ for a solution with $Ra = 45\,000$, $q = 1$, $E = 10^{-4}$, $\lambda = 0.05$, $M = 4$. The colour shows the vertical component of flow, arrows show the horizontal.

vertically outwards along the rotation axis, and returning in the vicinity of the tangent cylinder. Both of these components of flow are rather consistent in form, and both appear important for the dynamo action obtained, as is discussed in § 4. The magnetic field is somewhat more variable, but structures similar to those seen in figure 5 are very common. The zonal field, B, is characterized by two oppositely signed (and equatorially antisymmetric) patches in each hemisphere, located on and above the inner core. The lines of force of the meridional field, $Ar\sin\theta$, tend to form a single dominant (symmetric) structure in the interior, albeit with a somewhat complicated morphology on the inner core boundary; near to the surface (where the field is weaker), a secondary region of reversed polarity is common. It is interesting to note that such a morphology (with two poloidal polarities) was observed in the original calculations of Glatzmaier & Roberts (1995*a*, *b*), but not in their later models. The precise reason for this difference between the various models is unclear.

4. Dynamo mechanisms

The axisymmetric flow pattern described in § 3 proves robust, and is one of the strongest characteristics of this type of solution. This part of the flow can be understood in purely hydrodynamic terms. With the axisymmetric velocity separated into toroidal (v) and poloidal (ψ) parts,

$$\mathbf{u} = v\mathbf{e}_\phi + \nabla \times (\psi \mathbf{e}_\phi), \tag{4.1}$$

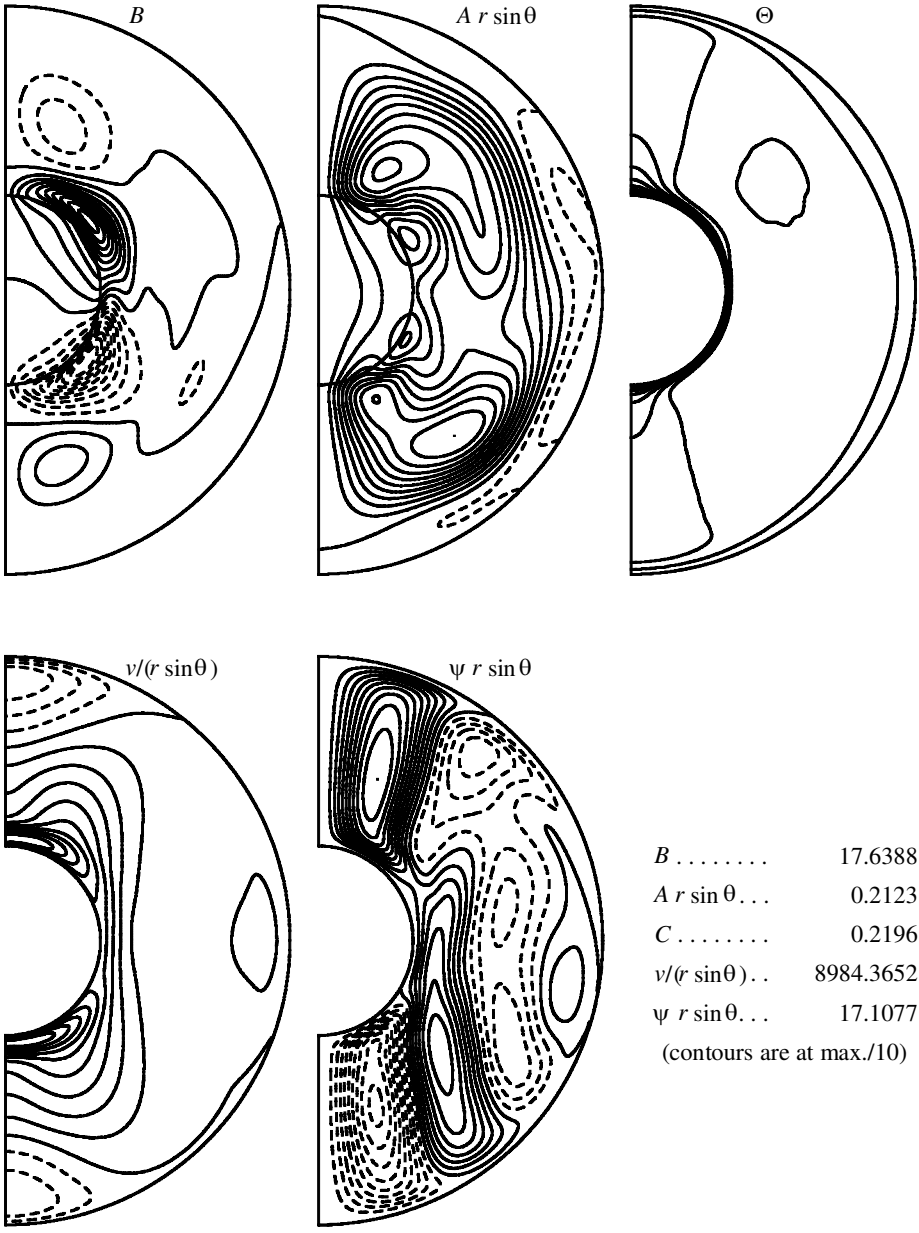

B	17.6388
$A\,r\sin\theta$ . . .	0.2123
C	0.2196
$v/(r\sin\theta)$ . .	8984.3652
$\psi\ r\sin\theta$ . . .	17.1077

(contours are at max./10)

Figure 5. Axisymmetric fields in a meridional plane, for a solution with $Ra = 45\,000$, $q = 1$, $E = 10^{-4}$, $\lambda = 0.05$, $M = 4$. B gives the zonal magnetic field, $Ar\sin\theta$ the meridional lines of force, Θ the temperature, $v/(r\sin\theta)$ the zonal angular velocity, and $r\sin\theta$ the meridional streamfunction.

the non-magnetic momentum equation gives

$$\frac{\partial v}{\partial z} = qRa\frac{1}{r}\frac{\partial \Theta}{\partial \theta} + E(D^2)^2\psi, \tag{4.2}$$

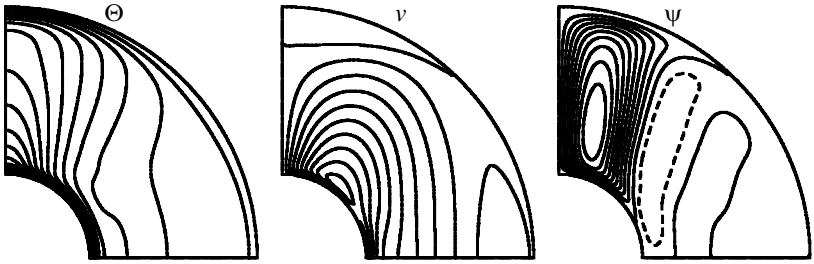

Figure 6. The three hydrodynamic axisymmetric variables Θ, v and ψ, in a meridional plane, for a typical equatorially symmetric, non-magnetic solution, showing the basic thermal wind state. From calculations with $Ra = 30\,000$, $q = 1$, $E = 10^{-4}$, $\lambda = 0.05$, $M = 1$.

$$\frac{\partial \psi}{\partial z} = -ED^2 v, \tag{4.3}$$

where $D^2 = (\nabla^2 - s^{-2})$, in terms of cylindrical radius, $s = r \sin\theta$.

For a highly supercritical system such as the present, strong non-axisymmetric convection outside the tangent cylinder results in highly efficient heat transport there, so that this outer region becomes relatively well-mixed, with a comparatively low mean temperature (close to that of the outer boundary), and a strong thermal boundary layer at the inner core. In comparison, the geometry of the polar regions (inside the tangent cylinder) hinders this development, and the thermal boundary layer is weaker there, with a relatively strong radial temperature gradient remaining in the bulk fluid. This results in a characteristic temperature profile such as that shown in figure 6 (for a calculation with equatorial symmetry imposed, and slightly less strongly driven, but otherwise similar to those described before).

This gives a characteristic gradient $\partial\Theta/\partial\theta$, negative (in the Northern Hemisphere) in the vicinity of the tangent cylinder. By equation (4.2), this must in the main be balanced by a negative gradient $\partial v/\partial z$. (Since the Ekman number is small, the viscosity term is negligible to first order.) No-slip conditions impose $v = 0$ at the outer boundary, so we anticipate $v > 0$ in the interior. Since the inner core is free to rotate, v can be non-zero at the inner core boundary, and the solution takes advantage of this option, with the inner core spinning up to a velocity close to that of the adjacent fluid via the viscous torque.

In equation (4.3), there are no first order terms capable of balancing $\partial\psi/\partial z$ in the bulk fluid, and so ψ is relatively z-independent in the interior. Near the boundaries, however, large gradients occur, and viscosity cannot be neglected. Gradients are strongest near the inner core boundary, where $D^2 v$ is strongly negative (as can be deduced from the strong local maximum). The ensuing positive gradient in $\partial\psi/\partial z$ gives rise to the positive ψ within the tangent cylinder. $\psi = 0$ is required at the outer boundary, and it is in accommodating this requirement—and hence requiring $D^2 v > 0$ (a local minimum) near the boundary where $v = 0$—that the polar negative in the toroidal flow is required.

The resultant picture—with negative (westward) flow near the polar axis at the surface, positive (eastward) toroidal flow near the axis at depth, and with meridional circulation outwards along the axis, returning along the tangent cylinder—is exactly that evident in figure 5, and is extremely robust, a similar pattern being obtained with or without magnetic fields, as will be seen. It is the viscous stress on the inner core,

associated with the toroidal flow, which drives the strong inner core superrotation, described in detail by Sarson & Jones (1999).

This characteristic toroidal velocity is also very important for the associated dynamo action. If the axisymmetric magnetic field is also written in toroidal (B) and poloidal (A) parts,

$$\mathbf{B} = B\mathbf{e}_\phi + \nabla \times (A\mathbf{e}_\phi), \tag{4.4}$$

then the axisymmetric induction equation gives

$$\frac{\partial B}{\partial t} + s\nabla \times (\psi \mathbf{e}_\phi) \cdot \mathrm{grad}\left(\frac{B}{s}\right) = D^2 B + s\nabla \times (A\mathbf{e}_\phi) \cdot \mathrm{grad}\left(\frac{v}{s}\right) + \mathbf{e}_\phi \cdot (\nabla \times \mathcal{E}), \tag{4.5}$$

$$\frac{\partial A}{\partial t} + \frac{1}{s}\nabla \times (\psi \mathbf{e}_\phi) \cdot \mathrm{grad}(sA) = D^2 A + \mathbf{e}_\phi \cdot \mathcal{E}, \tag{4.6}$$

where $\mathcal{E}$ is the axisymmetric part of $(\mathbf{u} \times \mathbf{B})$ arising from non-axisymmetric $\mathbf{u}$ and $\mathbf{B}$. The second to last term in equation (4.5), allowing for the generation of toroidal field from poloidal via differential rotation ($\mathrm{grad}(v/s)$), is the well-known ω-effect (Roberts 1994). This term is responsible for the strong axisymmetric zonal field evident in figure 5.

The axisymmetric poloidal field must itself be generated by the non-axisymmetric convection via the so-called α-effect, relying upon the quantity $\mathcal{E}$ in equation (4.6). This term is necessary for dynamo action, since A cannot be sustained by the purely axisymmetric (linear) terms in this equation (Roberts 1994). These solutions do not seem to have difficulty with this constraint, however; the strong three-dimensional velocities arising in the vicinity of the tangent cylinder (figure 4) generate a strong axisymmetric poloidal field there (figure 5). (In fact, axisymmetric poloidal field is generated by non-axisymmetric convection throughout the outer core; it is typically strongest near the inner core, however, where both the toroidal field and the convection—driven by the imposed heat flux at the inner core boundary—are strongest.) It is clear, in any case, that the axisymmetric toroidal field is dominantly produced by the differential rotation, so that the dynamo is better approximated as of $\alpha\omega$ type (cf. the 'Busse–Zhang' like solutions of Olson *et al.* (1999), which, they argue, are essentially of α^2 type; that is, the quantity $\mathcal{E}$ plays an essential role in equation (4.5) for their solutions, while the differential rotation does not.)

As noted above, the basic form of the axisymmetric velocity is extremely robust. This can clearly be seen in figure 7, where the differential rotation and poloidal streamfunction are shown for typical solutions obtained for $\mathbf{B} \neq \mathbf{0}$ and for $\mathbf{B} = \mathbf{0}$ (i.e. for one normal dynamo solution, and for one solution where the magnetic field has been switched off). The plots show the same characteristic form for both quantities, differing only in the typical magnitudes. Differential rotation is stronger with no magnetic field present; the magnetic field in a normal dynamo solution reduces this quantity considerably. This can be seen in plots of the axisymmetric Lorentz force, which consistently show a strongly negative azimuthal force opposing the dominant zonal flow above the inner core. This is clearly consistent with the results reported by Sarson & Jones (1999), that the principal effect of the magnetic torque on the inner core is to act as a 'braking torque', reducing the inner core rotation rate from its non-magnetic value.

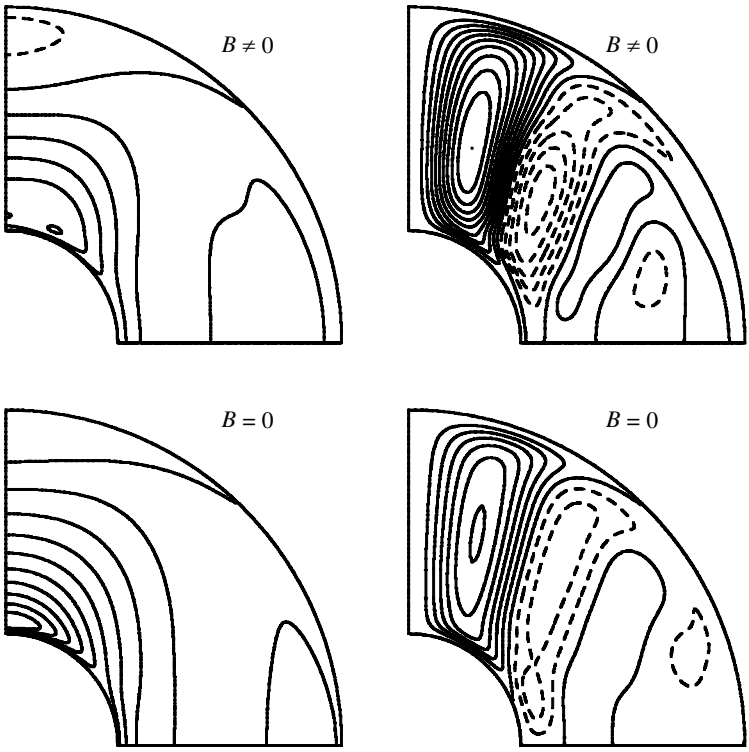

Figure 7. Zonal angular velocity, $v/(r\sin\theta)$ (left), and meridional streamfunction, $\psi r\sin\theta$ (right), for typical solutions obtained with $|\mathbf{B}| \neq 0$ (top) and with $|\mathbf{B}| = 0$ (bottom). From calculations with $Ra = 30\,000$, $q = 1$, $E = 10^{-4}$, $\lambda = 0.05$, $M = 1$, with equatorial symmetry imposed. The same scale is used in comparable plots.

The relative simplicity of this effect offers one obvious explanation of the equilibration of these dynamos. In the non-magnetic case, the field has been artificially removed. If we restore a small magnetic field and let it develop kinematically—i.e. if we simply time-step the induction equation (2.2) with the non-magnetic velocity held fixed, rather than time-stepping the full set of equations (2.1)–(2.3) normally—then we obtain strong exponential field growth; this velocity is supercritical in terms of dynamo action. If we run the same experiment with the velocity from the equilibrated dynamo case, very weakly exponential behaviour is found; the velocity is marginal for dynamo action. This should be expected, of course. Any dynamically self-consistent system in a more-or-less steady state (at its natural, equilibrated, field-strength) must operate about criticality; otherwise the Lorentz force associated with a growing field will act on the fluid flow so as to inhibit continued growth. In the present case, the relatively simple reduction in the zonal velocity effected by the magnetic field offers a simple mechanism for understanding the equilibration. Since it is this component of flow that creates toroidal field via the ω-effect, the reduction of this flow will influence dynamo action in a direct way. The effect is akin to the 'ω-quenching' used in some nonlinear mean-field models, whereby this generation term is reduced as the field strength increases. A similar mechanism was discussed in some detail by Gilman (1983).

While the simplicity of this effect is appealing, and it clearly must contribute significantly towards equilibration, it would be misleading to insist that this need be the only mechanism present in these solutions. Although the non-axisymmetric flow appears to be relatively little affected by the field equilibration (convection remaining of comparable magnitude and form in either state), extremely subtle changes are often all that are required to change the stretching properties (essential for dynamo action) of a three-dimensional flow, and this may also be occurring in the present. Additionally, figure 7 shows that, as well as weakening the differential rotation, the Lorentz force acts to strengthen the meridional circulation. While we think this feature of the flow acts principally to affect the time-behaviour of these solutions, as discussed below, it may also influence the equilibration process. Nevertheless, the simple picture outline above—of a thermal wind flow co-existing with strong non-axisymmetric convection, generating the dominant toroidal magnetic field via the ω-effect, and being moderated by the Lorentz force to equilibrate dynamo action—goes a long way towards explaining the comparatively steady-state behaviour exhibited by our model at times.

In the kinematic experiments described above, where the evolution of magnetic field was investigated with the velocity held fixed, the exponential behaviour obtained was monotonic; solutions either grew or decayed, but did not change polarity. And while the above illustrations made use of calculations with equatorial symmetry imposed, and with $M = 1$, neither of these factors limit our conclusions; solutions in more general cases remain dominantly equatorially symmetric throughout most of their time-evolution, and the kinematic behaviour of typical states is similar. Equilibrated solutions of this type are clearly a good model for the generation of a predominantly steady dipole field, but not for a field subject to reversals.

One component of these solutions may have a very strong effect on the time-dependence, however: the meridional circulation. As shown above, a characteristic form of this type of flow is present in our solutions, both as a part of the basic thermal wind mechanism, and due to the action of the axisymmetric Lorentz force. Continual fluctuations in the strength of this component of flow occur, from fluctuations in both thermal and magnetic forces. The effect of meridional circulation on kinematic $\alpha\omega$ dynamo action has been well understood since the definitive study of Roberts (1972); when present in the appropriate magnitude and sense, it acts to enhance dynamo action, and to make the favoured mode stationary, where $\alpha\omega$ dynamos tend, in its absence, to favour oscillatory solutions. A decrease in the magnitude of meridional circulation might then cause a solution maintaining an essentially steady field to fluctuate, leading to parity reversal if the velocity remained altered in this way for an appropriate period of time. It might also be accompanied by a decrease in field strength, a characteristic suggested for many geomagnetic reversals.

The potential of such a mechanism to explain occasionally reversing behaviour was noted by Gubbins & Sarson (1994), after three-dimensional kinematic dynamo calculations confirmed the behaviour previously observed in $\alpha\omega$ systems. Sarson & Jones (1999), analysing a reversal of an $M = 1$ ($2\frac{1}{2}$-dimensional) solution of GR type, observed the field transition to be preceded by an obvious fluctuation in the meridional circulation, and suggested this as an instance where the reversal mechanism appears to have been applicable in a dynamical context. Kinematic calculations,

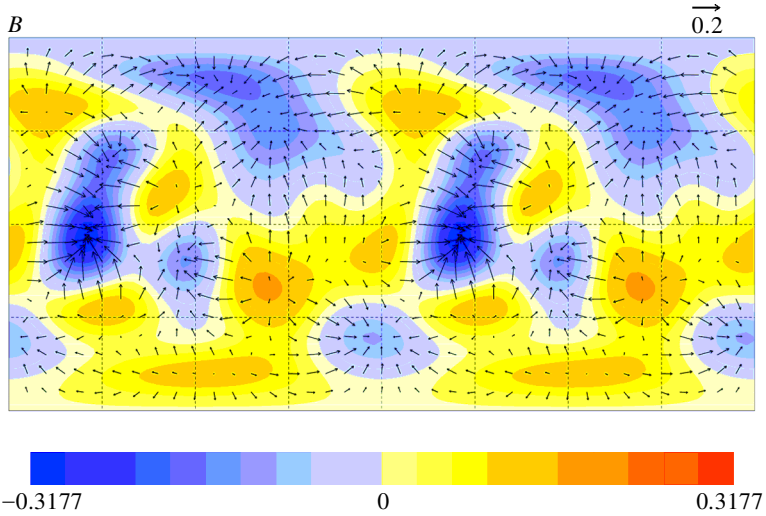

Figure 8. **B** on the surface of the dynamo region, for the solution with $Ra = 45\,000$, $q = 1$, $E = 10^{-4}$, $\lambda = 0.05$, $M = 4$, detailed in $x3$. The colour shows the radial component of field, arrows show the tangential.

investigating the dynamo action of GR flows with normal and reduced meridional circulations, and finding agreement with the kinematic behaviour outlined above, backed up this claim. Additional reversals of this type of solution have been studied for $M = 2$ and $M = 4$. The applicability of the kinematic reversal mechanism to these solutions, and to the geodynamo, is discussed in some detail in § 6. Regardless of its applicability in this specific instance, however, the general mechanism clearly remains feasible.

5. Geomagnetic diagnostics

Despite the caveats discussed in § 1, on the prematurity of any detailed comparison between numerical models and the geodynamo, it remains of some interest to compare some of the appropriate features.

Most simply, we can plot the external expression of our dynamo process, the magnetic field on the outer boundary, for comparison with historical field models downward-continued to the Earth's core–mantle boundary (CMB); this is done in figure 8, for the snapshot detailed in § 3. There are some features that bear comparison with the geodynamo. The field is typically dominated by the equatorially antisymmetric (dipole) symmetry, although deviations from pure symmetry are common (features are typically stronger in one hemisphere than in the other). The main flux lobes of the dipole symmetry field are offset from the poles, typically at latitudes of 60–70°, often with a reverse polarity patch at the pole itself; such features have been noted for the historical field (Gubbins & Bloxham 1987). The magnitude of the field in figure 8 is given in non-dimensional units. Rescaling appropriately for the Earth, using $\mathcal{B} \sim 2.2$ mT as described in § 3, gives peak surface values of the order of 0.7 mT, a value comparable with that of the present-day field. While the dominant wavelength of our solution, $m = 2$, also agrees with historical observations, this fac-

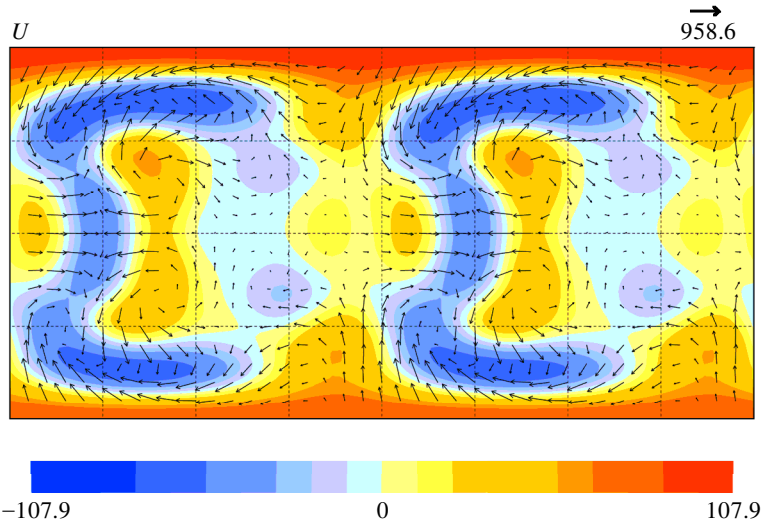

Figure 9. **U** just below the surface of the dynamo region (at $r = 1.45$), for the solution with $Ra = 45\,000$, $q = 1$, $E = 10^{-4}$, $\lambda = 0.05$, $M = 4$. The colour shows the radial component of flow, arrows show the tangential. The non-dimensional units of velocity give the local R_{m}.

tor is somewhat constrained by the base wavenumber used in this calculation, and it would be unwise to make too much of this fact.

Beyond the high-latitude dipole-symmetry field lobes, strong flux lobes also appear in the equatorial regions. These features show a weaker preference for pure equatorial symmetry, are typically smaller scale, and vary rather chaotically with time. Compared with similar features in the historical field, these lobes are often rather strong; in the snapshot shown, for example, the maximum surface field occurs in such a lobe.

The secular variation of this model has not been extensively studied, but surface features appear to drift both eastwards and westwards, with neither direction being obviously preferred. The surface field is also prone to changes in polarity, which are not reflected in the field deep within the core (and, hence, are not apparent in plots such as figure 2). The deep internal field permeates the inner core, and so cannot fluctuate too violently, being constrained to change by diffusion rather than advection; the inner core acts as a stabilizing influence, as made clear by Hollerbach & Jones (1993, 1995). The near-surface field is not so constrained, and experiences frequent fluctuations, which might correspond to geomagnetic excursions. While this is at odds with the traditional view of a predominantly stable field subject to only occasional reversals, it is not inconsistent with the picture proposed on the basis of recent palaeomagnetic data by Gubbins (1999); in this scenario, the field is indeed subject to frequent excursions, only some of which are reflected in the inner core field.

For our dynamo model, we are also able to plot the near-surface velocity field, a quantity that can be inferred from magnetic field observations, albeit non-uniquely and subject to various assumptions (see, for example, Bloxham & Jackson 1991). It is of interest to correlate the magnetic field with the velocity, and the latter is plotted in figure 9. The velocity tends more strongly towards equatorial symmetry than the magnetic field. A tendency for the magnetic flux to be concentrated where the

surface fluid downwells (evinced by convergent arrows and negative radial velocities) is apparent. This phenomenon is to be expected in fluids at high R_m (where diffusion is weak and the field tends to be advected with the flow (Roberts 1994)); it has been anticipated in interpretations of the observed geomagnetic field (Gubbins 1993), and observed in numerical dynamo calculations, both kinematic (Hutcheson & Gubbins 1994) and dynamic (Kageyama & Sato 1997; Kitauchi & Kida 1998; Sakuraba & Kono 1999; Olson *et al*. 1999).

The axisymmetric meridional circulation associated with the thermal wind mechanism is also evident in the polar regions of figure 9. This feature of the flow may contribute to the offset of the dominant flux lobes from the pole, by a high R_m mechanism similar to that outlined above. It should be noted, however, that this type of flow is not strong in most core flow inversions, and it should be borne in mind that this feature of our solution is rather dependent upon viscous effects, which will be weaker in the Earth than in our model.

The spectrum of mean surface magnetic energy is shown, in figure 10, for the same snapshot; the equivalent spectrum for the observed 1980 field is included for comparison. Here we use dimensionalized values, calculated as before, and the spectra are calculated as

$$R_l = (l+1)\sum_{m=0}^{l}(g_l^m)^2 + (h_l^m)^2, \tag{5.1}$$

where g_l^m, h_l^m are Gauss coefficients in the standard potential field description applicable outside the dynamo region, $\mathbf{B} = -\operatorname{grad} V$,

$$V = a\sum_l \left|\frac{a}{r}\right|^{l+1}\sum_{m=0}^{l}(g_l^m\cos m\phi + h_l^m \sin m\phi)\overline{P}_l^m(\cos\theta). \tag{5.2}$$

Here, a is the Earth's surface radius, and the $\overline{P}_l^m$ are Schmidt normalized Legendre functions. The plot has been truncated at degree $l = 20$, although our model goes out to $l = 48$. The general agreement between the two spectra is reassuring, although deviations clearly exist. Notably, our dipole ($l = 1$) component is somewhat too weak for the 1980 field (although it has recently been suggested that the historical field is abnormally strong (Juarez *et al*. 1998)). Conversely, we have too much magnetic energy in degrees $2 < l < 8$; this is perhaps not surprising, given the strong field structures apparent in figure 8.

In addition to these instantaneous measures of a typical snapshot of our field, we can attempt to compare aspects of our solution during a reversal transition. Several reversal sequences have been studied in detail, including one obtained for $M = 4$; the first reversal apparent in the time-sequence is shown in figure 2. As noted above, the surface field of this solution is rather variable with time, and this remains so during this transition, with many changes of polarity (rather than a single event) being observed. This is apparent in sequences of virtual geomagnetic poles (VGPs) throughout the transition; most sites show several equatorial crossings. This is of course highly site-dependent, as is to be expected given the relatively complex field morphology. Having plotted comparable VGP sequences for many other sites, and for several reversals, no particular trend in the VGP paths has been noted (although no real statistical analysis has been performed). This is not surprising, however,

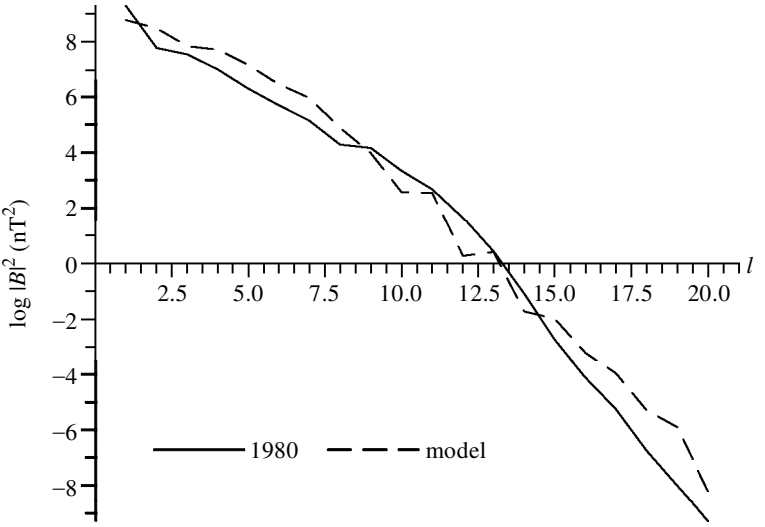

Figure 10. Surface field spectrum R_l, for the solution with $Ra = 45\,000$, $q = 1$, $E = 10^{-4}$, $\lambda = 0.05$, $M = 4$. The observed spectrum of the 1980 field is shown for comparison.

given the spherical symmetry of our basic model; any bias in VGP statistics in the palaeomagnetic record must be the result of inhomogeneities, probably at the CMB, as suggested by Laj *et al.* (1991). Local field intensities at individual sites during the transition also prove to be highly site-dependent, and display no obvious trends noted in the palaeomagnetic literature; local field strengths are not systematically decreased during the transition, for example.

6. Discussion

At the present time, detailed comparisons of numerical models with the geomagnetic record remain difficult. Numerical simulations of the dynamo, constrained to model the time-scales of the basic core MHD processes, arguably fail to satisfactorily model phenomena on both shorter and longer time-scales. All current dynamo models assume either geophysically inappropriate values of the fluid inertia or inappropriate ratios of inertia to viscosity, and either option will make much of the secular variation behaviour arising in these models inapplicable. (Although some authors argue that their output can be successfully scaled (Kuang & Bloxham 1998).) And, as discussed in § 1, time-series of sufficient length for comparison with the long-term palaeomagnetic record simply cannot currently be achieved.

Given the various strong numerical constraints, it is unclear whether either of these problems will be entirely overcome in direct numerical simulations, with any extrapolated future increase in computer power. A series of different models, investigating the different phenomena in different ways, may prove more fruitful. For secular variation behaviour, for example, a high-resolution solution, run for comparatively short total times, and assuming a mean field consistent with the longer time-scale models, may be worthwhile. For statistical studies of the long-term reversal behaviour, a parametrized model, incorporating the type of behaviour elucidated from direct MHD simulations into a greatly simplified system, may prove necessary.

In the meantime, however, direct simulations can still help us to understand the reversal (and other) behaviour of MHD dynamo systems in general; potentially useful comparisons with the Earth may still be made, although we should clearly not expect detailed agreement. The present work has focused on solutions of one simple numerical model, and tried to elucidate the important mechanisms occurring. These particular simulations are dominated by a thermal wind flow, and the differential rotation this imposes is responsible for the strong zonal magnetic fields that dominate the magnetic field. The system therefore broadly acts like an $\alpha\omega$-type dynamo (cf. α^2 type). The equilibration of dynamo action in this system also appears rather simple, with an 'ω-quenching' effect going a long way towards explaining this. In terms of the time-dependence of these solutions, the kinematic reversal mechanism noted by Sarson & Jones (1999) has been re-emphasized, whereby fluctuations in meridional circulation change the nature of the field preferentially excited, and lead to transitional episodes. Although the applicability of this kinematic mechanism to specific reversals of the dynamical system may be debated (and is further discussed below), the plausibility of the mechanism remains clear.

Despite being deduced from a model far from the appropriate parameter regime, many of these mechanisms may remain valid for the geodynamo. The strong zonal flow found in the thermal wind state might be expected to be a general feature of strongly supercritical convection in a spherical shell geometry, although the specific form determined here clearly remains viscously affected. Thus, differential rotation appears likely to play a significant role in the dynamo action of the Earth. The relatively simple equilibrated states found here may prove elusive in the geodynamo, however; in the absence of the balancing control of viscosity, much greater fluctuations in flow might be expected to occur with variations in the Lorentz force. The presence of meridional circulation in the geodynamo may also be rather different from that in our model. The thermal wind mechanism relies upon viscosity to drive this component of flow; in the geodynamo, the Lorentz force may be the dominant source. Greater fluctuations in behaviour might then be expected, if the meridional circulation is strongly dependent upon the magnetic field, and vice versa. In any event, relatively small amounts of this type of flow—from whatever source—can have a profound effect on dynamo action, and so the importance of this quantity for the time behaviour of the geodynamo remains great.

It should be noted here that our thermal wind flow—which underpins many of the dynamo mechanisms outlined—was calculated with an inner core free to rotate, and subject only to viscous and electromagnetic torques. The relevance of this case to the geodynamo is arguable. The equipotential gravity field arising from an inhomogeneous mantle will deform a stationary inner core from rotational symmetry, and strong gravitational torques will then act to restore it, if it is rotated from its equilibrium position (Buffett 1996). In such a model, the inner core is effectively locked in synchronous rotation with the mantle. Depending upon the inner core viscosity, however, it may be able to deform as it rotates, maintaining a surface topography in equilibrium with the mantle, yet still allowing net rotation of the order required (Buffett 1997). While such concerns clearly have a bearing on our model, and must be the subject of future study, they should not qualitatively affect the basic mechanisms. The locking of the inner core will not prevent strong zonal flows in the outer core fluid, and the greater shear necessary above the inner core, if the latter were indeed unable to co-rotate, might enhance

both the ω-effect and the generation of meridional circulation on which our model relies.

The meridional circulation reversal mechanism invoked by Sarson & Jones (1999) is not wholly original. The role of meridional circulation in changing the time-dependence of dynamo action—and the possibility of this explaining geomagnetic reversals—was noted rather early in the history of quantitative dynamo modelling; the ideas are present in Braginsky (1964*a*, *b*), albeit partly by analogy with Cartesian models. The generality of the effect of meridional circulation on spherical $\alpha\omega$ systems was firmly established by Roberts (1972), and the ensuing kinematic reversal mechanism is explicitly outlined in Parker (1979, p. 707), as follows.

> Suppose, for instance, that the distribution of shear and cyclones in the core of Earth is such that they cannot generate a stationary dipole... but there is more or less coincidentally a meridional flow of such a nature that the cyclones and shear are coerced into generating a stationary dipole. Then suppose that the meridional flow is interrupted or altered for a brief time. During that period the dynamo may generate an oscillatory field so that, when the meridional circulation is restored, the new stationary field may be reversed relative to the earlier stationary field. It is one more of the many theoretical possibilities for an occasional reversal of the geomagnetic field.

The healthy scepticism inherent in the final sentence is worth noting, particularly coming from one of the authors of an alternative kinematic mechanism (Parker 1969; Levy 1972*a*–*c*), based upon the migration of concentrations of shear or cyclone components of the velocity. While the fact that the meridional circulation mechanism appears to occur naturally in our dynamical system arguably makes it more than a theoretical possibility—and while the meridional circulation associated with the thermal wind flow may be more than 'coincidental'—it certainly remains only one of many possibilities. In addition to the alternative mechanism of Parker and Levy, fluctuations in the vigour of convection, leading to the kinematic excitation of secondary, symmetry-breaking modes, have also been posited as a kinematic reversal mechanism (Parker 1979). This latter effect may also be of relevance in our dynamical model, where equatorially symmetric fields are often significant during reversals, and where the vigour of convection (dependent upon Ra) clearly does influence reversal frequency. (By contrast, there is little evidence for migration of convective features in our model, as would support a Parker–Levy type model.)

It is perhaps unwise to lay too much stress on any kinematic mechanism in explaining the behaviour of such a dynamically fluctuating system. In our calculations, we track the time-evolution of several chaotically varying fields, and direct cause and effect are often difficult to isolate. In the reversal studied by Sarson & Jones (1999), for example, the background field intensity had already decreased somewhat before the proposed meridional circulation 'trigger' occurred. In light of the relationship between field strength and meridional circulation apparent in figure 7 (whereby strong fields enhance meridional circulation, presumably leading to greater field stability), the two effects may be rather intricately linked. This effect might also back up suggested correlations between field strengths and reversals (e.g Cox 1968), although, as noted in § 5, there is no real evidence for this in our calculations.

Additional transitions have been studied since Sarson & Jones (1999), for cases with $M = 2$ and $M = 4$. Although the later sequences certainly exhibit fluctuations in meridional circulation during transitions, the general behaviour is more chaotic—with several strong fluctuations in the outer core field occurring before the reversed polarity becomes firmly established in the inner core—and it is difficult to isolate any single critical events. It may be that these later reversals, obtained at $Ra = 45\,000$, are simply too supercritical to allow any simple analysis. Further analysis, and analysis of additional transitions (ideally less chaotic events), is clearly required. It might be noted, however, that this type of highly chaotic system fits well with the picture suggested by Gubbins (1999), of an outer core system prone to frequent fluctuations, which only occasionally succeed in reversing field throughout the core. (It should be re-emphasized here that the field we have been principally concerned with—in terms of both steady maintenance and reversals—is the main dynamo field, generated deep within the core, and subject to the stabilizing influence of the inner core observed by Hollerbach & Jones (1993, 1995). As noted in § 5, this field is not always reflected in the more variable surface field.)

In any event, the potential importance of meridional circulation to dynamo action is clear, and it remains one available tool in understanding reversal behaviour. It may contribute, for example, to the results of Glatzmaier *et al.* (1999), who investigated dynamo systems with a variety of imposed inhomogeneous CMB heat fluxes. They found that systems with greater polar heat fluxes, which might be expected to enhance the meridional circulation evident in our thermal wind flow, tended to be of rather stable polarity; conversely, systems with reduced polar heat fluxes (and, presumably, weakened polar circulation) were abnormally prone to reversal.

In a field that remains relatively little understood, much freedom for speculation exists. New observations may change our picture of the long-term behaviour of the geodynamo; e.g. the recent studies proposing significant changes in our understanding of the recent palaeomagnetic field (of the order of 1–5 Myr), in terms both of its field intensity (Juarez *et al.* 1998), and of the frequency of reversal/excursional events (Gubbins 1999). One could construct a theory linking the two phenomena: an abnormally strongly driven episode of convection might be responsible both for stronger mean intensities and more chaotic time-behaviour. Such speculation remains fruitless, however, until we have better constraints both on the behaviour of MHD dynamos, and on the past behaviour of the geomagnetic field; further work in both directions is required before we can claim to have a quantitative understanding of the Earth's reversal behaviour.

I thank Chris Jones and Keke Zhang for many helpful discussions over an extended period, and Steve Gibbons for the preparation of figure 1. This work was supported by the UK PPARC grant GR/K06495.

References

Bloxham, J. & Jackson, A. 1991 Fluid flow near the surface of earth's outer core. *Rev. Geophys.* **29**, 97–120.

Braginsky, S. I. 1964*a* Theory of the hydromagnetic dynamo. *Sov. Phys. JETP* **20**, 1462–1471. (Russian original 1964 *Zh. Eksp. Teor. Fiz.* (USSR), **47**, 2178.)

Braginsky, S. I. 1964*b* Kinematic models of the Earth's hydromagnetic dynamo. *Geomagn. Aeron.* **4**, 572–583. (Russian original 1964 *Geomagn. Aeron.* (USSR), **4**, 732.)

Buffett, B. A. 1996 A mechanism for decade fluctuations in the length of day. *Geophys. Res. Lett.* **23**, 3803–3806.

Buffett, B. A. 1997 Geodynamic estimates of the viscosity of the Earth's inner core. *Nature* **388**, 571–573.

Cox, A. 1968 Lengths of geomagnetic polarity intervals. *J. Geophys. Res.* **73**, 3247–3260.

Fearn, D. R. 1994 Nonlinear planetary dynamos. In *Lectures on solar and planetary dynamos* (ed. M. R. E. Proctor & A. D. Gilbert), pp. 219–244. Cambridge University Press.

Gilman, P. A. 1983 Dynamically consistent non-linear dynamos driven by convection in a rotating spherical-shell. 2. Dynamos with cycles and strong feedbacks. *Astrophys. J. Suppl.* **53**, 243–268.

Glatzmaier, G. A. & Roberts, P. H. 1995*a* A three-dimensional self-consistent computer simulation of a geomagnetic field reversal. *Nature* **377**, 203–209.

Glatzmaier, G. A. & Roberts, P. H. 1995*b* A three-dimensional convective dynamo solution with rotating and finitely conducting inner core and mantle. *Phys. Earth Planet. Interiors* **91**, 63–75.

Glatzmaier, G. A. & Roberts, P. H. 1996*a* An anelastic evolutionary geodynamo simulation driven by compositional and thermal convection. *Physica* D **97**, 81–94.

Glatzmaier, G. A. & Roberts, P. H. 1996*b* Rotation and magnetism of Earth's inner core. *Science* **274**, 1887–1891.

Glatzmaier, G. A. & Roberts, P. H. 1997 Simulating the geodynamo. *Contemp. Phys.* **38**, 269–288.

Glatzmaier, G. A., Coe, R. S., Hongre, L. & Roberts, P. H. 1999 The role of the Earth's mantle in controlling the frequency of geomagnetic reversals. *Nature* **401**, 885–890.

Gubbins, D. 1993 Geomagnetism and inferences for core motion. In *Flow and creep in the solar system: observations, modelling and theory* (ed. D. B. Stone & S. K. Runcorn), pp. 97–111. Dordrecht: Kluwer.

Gubbins, D. 1999 The distinction between geomagnetic excursions and reversals. *Geophys. J. Int.* **137**, F1–F3.

Gubbins, D. & Bloxham, J. 1987 Morphology of the geomagnetic field and implications for the geodynamo. *Nature* **325**, 509–511.

Gubbins, D. & Sarson, G. 1994 Geomagnetic field morphology and kinematic dynamos. *Nature* **368**, 51–55.

Hollerbach, R. & Jones, C. A. 1993 Influence of the Earth's inner core on geomagnetic fluctuations and reversals. *Nature* **365**, 541–543.

Hollerbach, R. & Jones, C. A. 1995 On the magnetically stabilizing role of the Earth's inner core. *Phys. Earth Planet. Interiors* **87**, 171–181.

Hutcheson, K. A. & Gubbins, D. 1994 Kinematic magnetic field morphology at the core mantle boundary. *Geophys. J. Int.* **116**, 304–320.

Jacobs, J. A. 1994 *Reversals of the Earth's magnetic field*. Cambridge University Press.

Jones, C. A., Longbottom, A. W. & Hollerbach, R. 1995 A self-consistent convection driven geodynamo model, using a mean field approximation. *Phys. Earth Planet. Interiors* **92**, 119–141.

Juarez, M. T., Tauxe, L., Gee, J. S. & Pick, T. 1998 The intensity of the Earth's magnetic field over the past 160 million years. *Nature* **394**, 878–881.

Kageyama, A. & Sato, T. 1997 Generation mechanism of a dipole field by a magnetohydrodynamic dynamo. *Phys. Rev.* E **55**, 4617–4626.

Kitauchi, H. & Kida, S. 1998 Intensification of magnetic field by concentrate-and-stretch of magnetic flux lines. *Phys. Fluids* **10**, 457–468.

Kuang, W. & Bloxham, J. 1998 Numerical dynamo modelling: comparison with the Earth's magnetic field. In *The core–mantle boundary region* (ed. M. Gurnis, M. E. Wysession, E. Knittle & B. A. Buffett), pp. 97–208. Washington, DC: American Geophysical Union.

Laj, C., Mazaud, A., Weeks, R., Fuller, M. & Herrero-Bervera, E. 1991 Geomagnetic reversal paths. *Nature* **351**, 447.

Langereis, C. G., Dekkers, M. J., de Lange, G. J., Paterne, M. & van Santvoort, P. J. M. 1997 Magnetostratigraphy and astronomical calibration of the last 1.1 Myr from an eastern Mediterranean piston core and dating of short events in the Brunhes. *Geophys. J. Int.* **129**, 75–94.

Levy, E. H. 1972*a* Effectiveness of cyclonic convection for producing the geomagnetic field. *Astrophys. J.* **171**, 621–633.

Levy, E. H. 1972*b* Kinematic reversal schemes for the geomagnetic dipole. *Astrophys. J.* **171**, 635–642.

Levy, E. H. 1972*c* On the state of the geomagnetic field and its reversals. *Astrophys. J.* **175**, 573–581.

Lund, S. P., Acton, G., Clement, B., Hastedt, M., Okada, M. & Williams, R. 1998 Geomagnetic field excursions occurred often during the last million years. *Eos* **79**, 178–179.

Olson, P., Christensen, U. & Glatzmaier, G. A. 1999 Numerical modeling of the geodynamo: mechanisms of field generation and equilibration. *J. Geophys. Res.* B **104**, 10 383–10 404.

Parker, E. N. 1969 The occasional reversal of the geomagnetic field. *Astrophys. J.* **158**, 815–827.

Parker, E. N. 1979 *Cosmical magnetic fields*. Oxford: Clarendon.

Roberts, P. H. 1972 Kinematic dynamo models. *Phil. Trans. R. Soc. Lond.* A **271**, 663–697.

Roberts, P. H. 1994 Fundamentals of dynamo theory. In *Lectures on solar and planetary dynamos* (ed. M. R. E. Proctor & A. D. Gilbert), pp. 1–58. Cambridge University Press.

Sakuraba, A. & Kono, M. 1999 Effect of the inner core on the numerical solution of the magnetohydrodynamic dynamo. *Phys. Earth Planet. Interiors* **111**, 105–121.

Sarson, G. R. & Jones, C. A. 1999 A convection driven geodynamo reversal model. *Phys. Earth Planet. Interiors* **111**, 3–20.

Sarson, G. R., Jones, C. A. & Longbottom, A. W. 1998 Convection driven geodynamo models of varying Ekman number. *Geophys. Astrophys. Fluid Dyn.* **88**, 225–259.

Zhang, K. & Jones, C. A. 1997 The effect of hyperviscosity on geodynamo models. *Geophys. Res. Lett.* **24**, 2869–2872.

Zhang, K., Jones, C. A. & Sarson, G. R. 1998 The dynamical effects of hyperviscosity on numerical geodynamo models. *Studia Geophysica et Geodaetica* **42**, 247–253.